ACS APPLIED MATERIALS & INTERFACES

Research Article

Cite This: ACS Appl. Mater. Interfaces XXXX, XXX, XXX−XXX

www.acsami.org

Protection of $GaInP_2$ Photocathodes by Direct Photoelectrodeposition of MoS_x Thin Films

Mitchell Lancaster,[†] Rachel Mow,[§] Jun Liu,[§] Quintin Cheek,[†] Molly M. MacInnes,[†] Mowafak M. Al-Jassim,[§] Todd G. Deutsch,[§] James L. Young,[§] and Stephen Maldonado*[,†,‡]

[†]Department of Chemistry and [‡]Program in Applied Physics, University of Michigan, 930 N. University Ave., Ann Arbor, Michigan 48109-1055, United States

[§]National Renewable Energy Laboratory, 15013 Denver West Pkwy, Golden, Colorado 80401, United States

Supporting Information

ABSTRACT: Catalytic MoS_x thin films have been directly photoelectrodeposited on $GaInP_2$ photocathodes for stable photoelectrochemical hydrogen generation. Specifically, the MoS_x deposition conditions were controlled to obtain 8−10 nm films directly on p-$GaInP_2$ substrates without ancillary protective layers. The films were nominally composed of MoS_2, with additional MoO_xS_y and MoO_3 species detected and showed no long-range crystalline order. The as-deposited material showed excellent catalytic activity toward the hydrogen evolution reaction relative to bare p-$GaInP_2$. Notably, no appreciable photocurrent reduction was incurred by the addition of the photoelectrodeposited MoS_x catalyst to the $GaInP_2$ photocathode under light-limited operating conditions, highlighting the advantageous optical properties of the film. The MoS_x catalyst also imparted enhanced durability toward photoelectrochemical hydrogen evolution in acidic conditions, maintaining nearly 85% of the initial photocurrent after 50 h of electrolysis. In total, this work demonstrates a simple method for producing dual-function catalyst/protective layers directly on high-performance, planar III−V photoelectrodes for photoelectrochemical energy conversion.

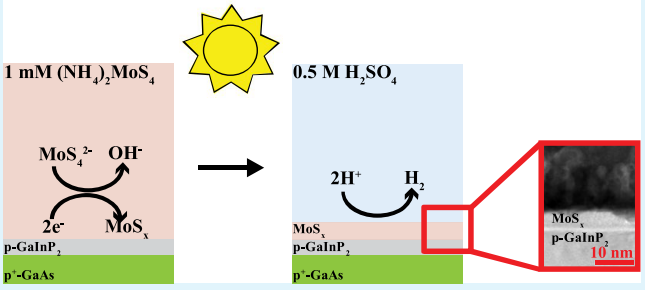

KEYWORDS: *photoelectrodeposition, III−V semiconductor, MoS_x, water-splitting, durability*

INTRODUCTION

Direct conversion of solar energy to hydrogen utilizing aqueous electrolytes offers a promising means of producing an energy-dense, storable, and renewable fuel. Despite great interest in photoelectrochemical energy conversion over the past several decades, systems demonstrating stable, high current densities with sufficient photovoltage to split water have yet to emerge. One attractive photoelectrode material for hydrogen production is p-type $GaInP_2$.[1−4] $GaInP_2$ has a nearly optimal bandgap (∼1.8 eV)[1,5,6] and can be integrated with lower band gap bottom absorbers (e.g., GaAs or GaInAs) to produce large photovoltages appropriate for unbiased water photoelectrolysis.[5,7−10] However, the propensity for p-$GaInP_2$ to corrode in aqueous electrolytes and the relativity poor native electrocatalytic activity for H^+ reduction are key barriers for use in renewable hydrogen generation technologies.[11−15]

Numerous coating strategies have been explored and developed for improving semiconductor interface durability including sputtering,[16−18] atomic layer deposition (ALD),[19−22] spin-coating,[23,24] and (photo)electrodeposition.[25−27] For $GaInP_2$ photocathodes, the combination of an ALD-TiO_2 protective layer and a molecular catalyst improved the short-term stability and catalytic activity of the photoelectrode.[19] However, the durability of this interface under light-limited operating conditions past 20 h remains unclear. More recently, a dual catalyst/protective layer design was employed during the deposition of MoS_2 on p-$GaInP_2$.[16] A two-step method of sputtering Mo followed by sulfidization produced an active layer that improved the stability and was more electrocatalytic toward hydrogen evolution. Nevertheless, limited control of the sulfidization process led to unconverted elemental Mo that significantly decreased the observed photocurrent.

Low-temperature photoelectrodeposition offers several unique advantages for the preparation of dual purpose (stabilization and electrocatalyst) protective layers on photoelectrodes. First, deposition rates can be precisely controlled by manipulation of the applied current or bias, allowing high fidelity over the deposit thickness. Second, low temperatures prevent interdiffusion and surface phase segregation, common problems for III−V semiconductors subjected to higher temperatures.[28−30] Third, electrochemical equipment needed for photoelectrodeposition are simple and low cost relative to the infrastructure needed for vacuum-based depositions.

Received: February 28, 2019
Accepted: June 18, 2019
Published: June 18, 2019

DOI: 10.1021/acsami.9b03742
ACS Appl. Mater. Interfaces XXXX, XXX, XXX−XXX

In this work, the direct photoelectrodeposition of MoS_x thin films on p-$GaInP_2$ photocathodes is reported, and the resulting photoelectrochemical properties are detailed. These earth-abundant catalysts have shown excellent catalytic activity and stability for hydrogen evolution,[31−34] but direct photoelectrodeposition on a planar, III−V photoelectrode surface has not been described. Specifically, the results from MoS_x photoelectrodeposition experiments directly on p-$GaInP_2$ are discussed, including the photoelectrodeposition conditions necessary to produce uniform, thin MoS_x films. Additionally, the structure and composition of these films are detailed and presented in context to the catalytic, optical, and photoelectrochemical properties. Finally, the enhanced stability of the coated p-$GaInP_2$ photoelectrodes relative to the bare material is shown.

EXPERIMENTAL SECTION

Chemicals and Materials. Ammonium tetrathiomolybdate (Acros, 99.95%), potassium sulfate (Acros, >99%), sulfuric acid (OmniTrace, EMD Millipore), and Triton X-100 (EMD Millipore) were used as received. All solutions were made with >18 MΩ·cm resistivity water (Milli-Q). Zn-doped p-$GaInP_2$ epilayers with nominal thicknesses of 1 μm and 1×10^{17} cm^{-3} dopant density were grown by metalorganic vapor phase epitaxy on p^+-GaAs(100) substrates, miscut 2° toward (110), as described elsewhere.[5] Run numbers for each epilayer are provided in the Supporting Information. Electroplated gold was used to form an ohmic contact to the GaAs substrate.

MoS_x Deposition. $GaInP_2$ epilayers were diced and etched in 18 M sulfuric acid for 1 min before placing in an open-air, custom Teflon cell and sealing with a Viton o-ring. A three-electrode configuration with a Ag/AgCl (3 M KCl) reference (0.204 V vs normal hydrogen electrode (NHE)) and a graphite counter electrode was utilized. The electrolyte consisted of 0.001 M ammonium tetrathiomolybdate ($(NH_4)_2MoS_4$) and 0.5 M potassium sulfate (K_2SO_4). Deposition occurred under 50 mW cm^{-2} fiber optic illumination (ThorLabs), as measured with a 1.81 eV band gap $GaInP_2$ reference cell calibrated to an AM 1.5G spectrum. The current was applied via a SP-300 potentiostat (BioLogic) in a custom-built, dark Faraday cage. Post-deposition, electrodes were placed on glass slides, contacted to conductive copper tape via silver print (GC Electronics), and sealed with epoxy (Loctite EA E-120HP) for photoelectrochemical characterization (see inset of Figure S4 for an image of an electrode).

Voltammetry and Durability. Linear sweep voltammetry was collected with a Solartron 1287 electrochemical interface at a scan rate of 50 mV s^{-1}. All data are shown in "polarographic" convention, with positive currents indicating cathodic processes. The samples were illuminated with a 300 W Xenon arc lamp (Newport) through a AM 1.5G filter (Oriel) outputting an incident photon intensity equivalent to 100 mW cm^{-2}, as calibrated with the $GaInP_2$ reference cell. A single compartment, open-air quartz cell (Starna) containing 0.5 M H_2SO_4 and 0.001 M Triton X-100 held the MoS_x/$GaInP_2$ sample in the center, flanked by a Hg/$HgSO_4$ reference electrode (Koslow Scientific) containing a 0.5 M H_2SO_4 filling solution (0.687 V vs NHE) and a large-area Pt foil counter electrode on either side. Similarly, durability measurements were conducted in the same cell without Triton X-100 using a 250 W tungsten-halogen lamp (Oriel) with an infrared-blocking water filter (Newport). The H_2SO_4 electrolyte was refilled as needed over the course of the durability measurements. All potentials were measured/applied in a three-electrode configuration and are reported with respect to the reversible hydrogen electrode (Conversion provided in the Supporting Information).

External Quantum Yield and Reflectance. Quantum yield (incident photon-to-current efficiency) measurements were made between 300 and 700 nm at 10 nm intervals with a Newport 300 W xenon arc lamp and a SpectraPro 150 monochromator (Acton Optics). The electrode potential was held at −0.3 V vs E(RHE) with the photocurrents collected under 2 s light and 2 s dark intervals measured by a VersaStat 4 potentiostat (Princeton Applied Research) and read on a computer, controlled by custom LabVIEW software. The monochromator output intensity at each wavelength was separately measured by a calibrated Si photodiode. Reflectance measurements were acquired in air on a Cary 6000i spectrophotometer (Agilent) equipped with an integration sphere using an incidence angle normal to the electrode surface.

Electron Microscopy. Scanning electron micrographs were obtained on a JEOL-7800FLV microscope equipped with a Schottky-type field emission source and an Everhart−Thornley detector at an accelerating voltage of 10 kV. Corresponding elemental mapping was collected via an Oxford XMaxN energy-dispersive spectrometer. Scanning transmission electron micrographs were obtained with a FEI Tecnai F20 TEM equipped with a Gatan Enfinium EELS spectrometer and GIF Quantum K2 system at an accelerating voltage of 200 kV. The semicollection angle was 16 mrad. An energy shift of 120 eV and a dispersion of 0.25 eV per channel were employed to obtain a strong signal-to-noise ratio. Electron energy loss (EEL) spectra in scanning transmission electron microscopy (STEM) mode were recorded with a CCD camera. The acquisition time for each pixel was 0.5 s, and the total acquisition time was 23 min. The pixel size was 1.4 nm^2. A Pd/Au capping layer was deposited on the sample via sputtering to prevent surface damage during TEM sample preparation. The TEM lamella was prepared by standard focused ion beam lift-out techniques followed by Ga ion milling to reduce the final thicknesses to less than 100 nm.

X-ray Photoelectron Spectroscopy (XPS). X-ray photoelectron (XP) spectra were collected with a Kratos AXIS Ultra system operating at base pressures below 10^{-9} torr with a monochromatic Al Kα source (1486.6 eV). Pass energies of 160 and 20 eV were used to obtain survey and high-resolution spectra, respectively. Using CasaXPS software, a Shirley-type background correction was applied to the obtained spectra. Binding energies were calibrated to the binding energy for adventitious carbon (284.6 eV),[35] and peak intensities were normalized to that of the Mo $3d_{5/2}$ peak at 229.14 eV. Peak shapes were set to GL(30), i.e., 30% Gaussian and 70% Lorentzian. For fitting of Mo 3d spectra, peak separation between Mo $3d_{5/2}$ and $3d_{3/2}$ doublets was set to 3.1 eV.[36] Peak areas ratios were defined by spin-orbit coupling. The full width at half maximum for every peak of the same element was constrained to be the same. For quantification, relative sensitivity factors from the Kratos library were imported into CasaXPS.

Raman Spectroscopy. Raman spectra were collected on a Renishaw inVia microscope using a Nikon 20× objective (NA = 0.35) without any additional polarizing excitation/collection optical elements. A 532 nm laser was used as an excitation source with an incident power of 35 mW over ∼3 μm^2. For annealed samples, annealing was performed in a custom-built tube furnace at 550 °C under a steady flow (100 sccm) of argon (99.998%, Metro Welding Supply).

RESULTS

MoS_x Photoelectrodeposition. Figure 1a highlights the voltammetric responses of bare p-$GaInP_2$ in 0.5 M K_2SO_4 with and without 0.001 M of the MoS_x precursor, $(NH_4)_2MoS_4$. In the absence of illumination, no appreciable current was observed in the potential range of 0.6 to −0.4 V. Illuminating the electrode with 50 mW cm^{-2} of white light introduced two distinct features. First, a small peak at 0.3 V was observed, consistent with the reduction of surface oxides on p-$GaInP_2$.[13] Second, a large increase in the cathodic current beginning at 0.1 V was observed for hydrogen evolution. With 0.001 M of the MoS_x precursor added to the solution at the same light intensity, a large positive shift in the photocurrent onset was noted, and the light-limited plateau current was attenuated by the deep red solution color. The first voltammetric wave corresponded to the reduction of MoS_4^{2-}[37]

DOI: 10.1021/acsami.9b03742
ACS Appl. Mater. Interfaces XXXX, XXX, XXX−XXX

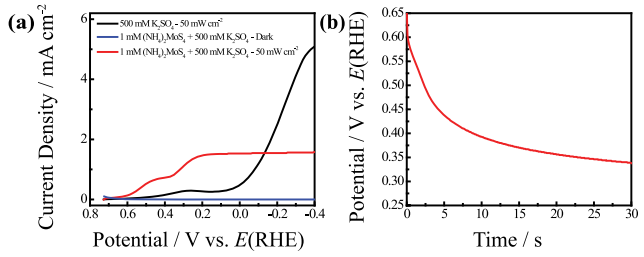

Figure 1. (a) Voltammetric responses of a bare p-$GaInP_2$ epilayer in 0.5 M K_2SO_4 under 50 mW cm^{-2} illumination (black), in 0.001 M $(NH_4)_2MoS_4$ + 0.5 M K_2SO_4 in the dark (blue), and in 0.001 M $(NH_4)_2MoS_4$ + 0.5 M K_2SO_4 under 50 mW cm^{-2} illumination (red). Scan rate: 50 mV s^{-1}. (b) Potential transient for the galvanostatic deposition of MoS_x thin films on p-$GaInP_2$ under 50 mW cm^{-2} illumination. Applied current density: 0.3 mA cm^{-2}.

$$MoS_4^{2-} + 2e^- + 2H_2O \rightarrow MoS_2 + 2SH^- + 2OH^- \quad (1)$$

however, no change in the electrode appearance was observed by eye. Similarly, cycling the electrode without illumination in the precursor solution from 0.6 to −0.4 V resulted in no alteration of the electrode appearance.

A galvanostatic deposition method was utilized to produce uniform thin films. Notably, potentiostatic depositions produced films with significant roughness and led to less reproducible thicknesses. Figure 1b shows a representative potential transient for a galvanostatic photoelectrodeposition of MoS_x on bare p-$GaInP_2$ at 0.3 mA cm^{-2} under 50 mW cm^{-2} illumination. After a rapid initial decrease from open-circuit potential, the electrode potential gradually drifted more negative until reaching a quasi-steady-state potential near 0.32 V. Although no distinct nucleation feature was observed in the transient, the voltammetry shown in Figure 1a suggests that the reduction of MoS_4^{2-} occurred at all potentials < 0.6 V, i.e., immediately after the charging current decay. A similar potential transient profile was also observed for longer depositions (Supporting Information, Figure S1).

Structure and Composition of Deposited MoS_x Films. Electron microscopy coupled with spectroscopic techniques was used to determine the film thickness, composition, and structure. A representative cross-section, bright-field scanning transmission electron microscopy (STEM) image of a film on p-$GaInP_2$ photoelectrodeposited at 0.3 mA cm^{-2} for 30 s under 50 mW cm^{-2} illumination in 0.001 M $(NH_4)_2MoS_4$ is shown in Figure 2a. An ∼8 nm-thick MoS_x film was observed between $GaInP_2$ and the Pd/Au capping layer deposited during STEM sample preparation. STEM analysis on multiple MoS_x films grown on separate $GaInP_2$ substrates under the same conditions produced film thicknesses ranging between 8 and 10 nm. An additional ∼0.75 nm-thick layer was consistently observed between the $GaInP_2$ substrate and the MoS_x film and attributed to a surface oxide. A longer deposition time of 2 min produced thicker films on the order of 40 nm (Supporting Information, Figure S1, inset). Figure 2b shows the corresponding dark-field image of the MoS_x. A sharp interface is apparent below the capping layer, indicating a nominally smooth top surface over the imaged area. Additional STEM/energy-dispersive spectrometry mapping (Supporting Information, Figure S2) showed a distinct diminution in the Ga, In, and P signals in the region of the film. Figure 2c highlights sulfur content in the films. The S EELS map in Figure 2c collected from the S $L_{2,3}$ edge at 165 eV confirmed that the films were sulfur-containing throughout. Analogous Mo mapping (Supporting Information, Figure S3b) was less clear on the absolute Mo content since the Mo M_3 and Mo M_2 edges strongly overlap with the tail of the C K edge (Supporting Information, Figure S3c). Nevertheless, the data were consistent that the as-deposited films were composed of S uniformly.

Separate assessment of the chemical oxidation states of Mo and S was performed via high-resolution XPS. High-resolution XP spectra (raw data, fits, and residuals) for the Mo 3d and S 2p regions are shown in Figure 3a,b (fitting details vide supra).

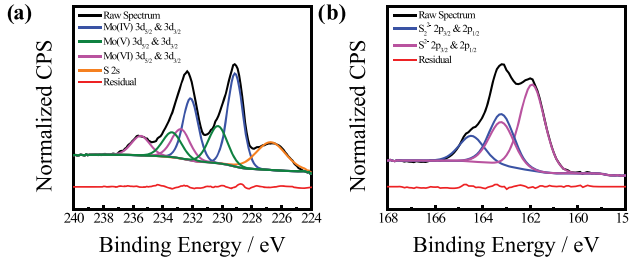

Figure 3. High-resolution (a) Mo 3d and (b) S 2p XP spectra of the as-deposited MoS_x thin film. Residuals are shown in red below the fitted spectra.

In Figure 3a, the Mo 3d region was composed of three Mo doublets corresponding to three different oxidation states: Mo(IV), Mo(V), and Mo(VI). In addition, a single peak at 226.9 eV was observed corresponding to an S 2s signal.[2,34] The Mo(IV) doublet and the S 2s signals suggest molybdenum disulfide.[2,34,36] The Mo(V) doublet was consistent with a ternary oxysulfide species (MoO_xS_y).[2,36,38] The doublet for Mo(VI) suggested that some molybdenum oxides (MoO_3) are also present.[2,34]

The S 2p spectrum in Figure 3b was fit to several different S oxidation states. The binding energies of these two sets of doublets were consistent with a mix of S^{2-} and S_2^{2-} anions present in MoS_x, widely reported for MoS_x materials with no

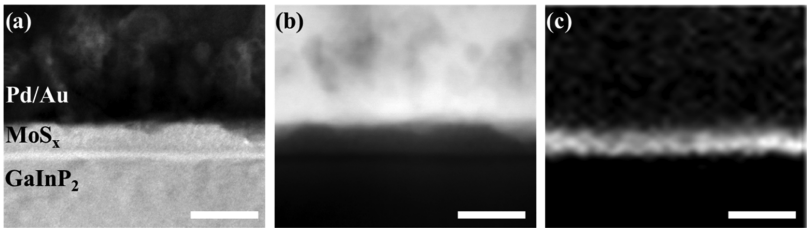

Figure 2. (a) Bright-field and (b) dark-field STEM images of the as-deposited MoS_x thin film and $GaInP_2$ interface. (c) Corresponding S $L_{2,3}$ edge EELS map of the MoS_x deposit and $GaInP_2$ interface. The sulfur signal is shown in white against a black background. Scale bars: 10 nm.

DOI: 10.1021/acsami.9b03742
ACS Appl. Mater. Interfaces XXXX, XXX, XXX−XXX

long-range structural order, i.e., amorphous.[2,34,36,38] Additionally, no elemental sulfur peaks were required to fit the S 2p spectrum. Combined, the relative intensities across Figure 3 suggested that a large portion of the film is composed of MoS_2. The quantification of the Mo and S spectra suggested an approximate Mo/S ratio of 1:1.6, corresponding to a majority MoS_2 makeup with some oxide/oxysulfide species present. As such, the films are collectively referred to as MoS_x.

Separate analyses were performed to ascertain the crystallinity of the MoS_x film. All X-ray diffraction measurements on the as-prepared film yielded no evidence of crystallinity, but the detection limit for the low total amount of material was not conclusive in this regard. Separate Raman analyses were performed to bolster this point. Raman spectra for bare p-$GaInP_2$, p-$GaInP_2$ with an as-deposited film, and p-$GaInP_2$ after film photoelectrodeposition and annealing for 30 min at 550 °C under Ar(g) are shown in Figure 4. For the bare

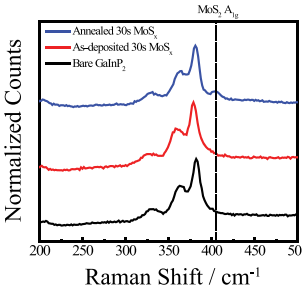

Figure 4. Raman spectra of a bare $GaInP_2$, as-deposited MoS_x/$GaInP_2$, and annealed MoS_x/$GaInP_2$ electrodes. The dashed line indicates the location of the A_{1g} mode of crystalline MoS_2.

sample, the three clear Raman peaks at 381, 364, and 330 cm^{-1} were observed, consistent with the two longitudinal optical phonon modes and one transverse optical phonon mode, respectively, for ordered $GaInP_2$.[39] The as-deposited sample shows an essentially identical spectrum, indicating that the as-deposited films showed no Raman signatures in this bandwidth. The Raman spectrum after annealing featured an additional small peak at 405 cm^{-1}. This signal was consistent with the A_{1g} mode of crystalline MoS_2.[40]

Photoelectrochemical Properties of the MoS_x/p-$GaInP_2$ Photocathode. The photoelectrochemical properties of p-$GaInP_2$ before and after film photoelectrodeposition are shown in Figure 5. Figure 5a shows the steady-state linear sweep voltammograms of p-$GaInP_2$ before and after film deposition when immersed in 0.5 M H_2SO_4 and 0.001 M Triton X-100 under AM 1.5G illumination. The reversible potential for H^+/H_2 is indicated by the vertical, dashed line. Several key differences in the voltammetry of the two electrodes are apparent. First, the onset potential for the hydrogen evolution reaction is shifted significantly. At a current density of 1 mA cm^{-2}, the potential of the coated electrode is 460 mV more positive than prior to film deposition. Next, the light-limited photocurrent density of the coated p-$GaInP_2$ electrode is essentially unchanged relative to the bare p-$GaInP_2$ electrode (11.7 vs 11.0 mA cm^{-2}, respectively). These features were consistent across two thin-film electrodes prepared from different p-$GaInP_2$ epilayers (with similar material properties as shown) (e.g., Supporting Information, Figure S4). Figure 5b shows representative external quantum yield measurements for p-$GaInP_2$ before and after film photoelectrodeposition. Despite a slight increase in the quantum yield at shorter wavelengths, there was no appreciable change in the quantum yield profile across the range of visible wavelengths. However, the reflectance data, depicted in Figure 5c, shows a measurable difference between the two types of electrodes. At all wavelengths shown, a 5–10% change in the reflectance was noted, with the largest differences occurring at shorter wavelengths.

Photoelectrochemical measurements recorded over longer periods of time were performed to assess the relative durability of the as-deposited coatings (Figure 6). Photocurrent–time measurements were performed for all electrodes under AM 1.5G illumination in the absence of any surfactant at an applied potential of 0 V vs E(RHE), i.e., under conditions where the photocurrent is light-limited for the MoS_x sample and near light-limited for the bare sample. Measurements at this potential allowed a direct comparison to several other reports of MoS_x/MoS_2-protected photocathodes (Supporting Information).[18,25] An additional durability measurement was performed at +0.25 V to assess the durability closer to the maximum power point. The photocurrent of the bare p-$GaInP_2$ electrode decayed quickly, reaching near zero within 3 h. After the photoelectrodeposition using the same conditions as for Figure 2, the photocurrent of the p-$GaInP_2$ photoelectrode was markedly more stable. At 0 V vs E(RHE), the electrode maintained 85% of the initial photocurrent over 50 h. Even after 100 h under light-limited conditions, 80% of the initial photocurrent was observed. The durability of a sample produced by the same 30 s photoelectrodeposition conditions at 0.25 V resulted in similar levels of stability over 50 h. P-type $GaInP_2$ electrodes coated with a film photoelectrodeposited for shorter times (10 s) still showed some improved durability

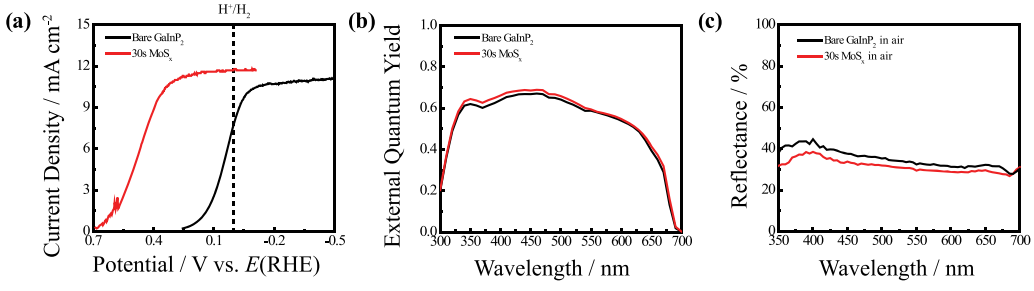

Figure 5. (a) Voltammetric responses of MoS_x/p-$GaInP_2$ and bare p-$GaInP_2$ photocathodes in 0.5 M H_2SO_4 + 0.001 M Triton X-100 under AM 1.5G illumination. Scan rate: 50 mV s^{-1}. The dashed line indicates the reversible potential for the hydrogen evolution reaction on this scale. (b) External quantum yield measurements for the same electrodes in 0.5 M H_2SO_4. Applied bias: −0.3 V vs E(RHE). (c) Reflectance measurements of MoS_x/p-$GaInP_2$ and bare p-$GaInP_2$ electrodes acquired without the electrolyte.

DOI: 10.1021/acsami.9b03742
ACS Appl. Mater. Interfaces XXXX, XXX, XXX–XXX

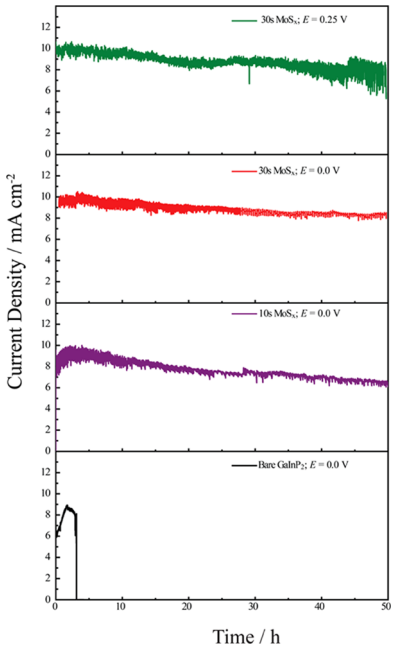

Figure 6. Durability measurements for bare p-$GaInP_2$, 10 s deposited MoS_x/p-$GaInP_2$, and 30 s deposited MoS_x/p-$GaInP_2$ photocathodes in 0.5 M H_2SO_4 under AM 1.5G illumination at an applied bias of either 0.0 or 0.25 V vs E(RHE).

over bare p-$GaInP_2$ but less stability than the films photoelectrodeposited for 30 s, losing 30% of the initial photocurrent density over 50 h of continuous operation.

DISCUSSION

The collective data supports three main points. First, photoelectrochemical reduction of $(NH_4)_2MoS_4$ on p-$GaInP_2$ is a straightforward route to obtain uniform coatings. The film material is disordered and results in negligible optical losses in the photoelectrochemical responses of p-$GaInP_2$. Second, the as-prepared films are electrocatalytic toward H^+ reduction. Third, such films impart enhanced durability to p-$GaInP_2$, similar to MoS_2 films deposited by vapor phase methods. These points are described below.

Photoelectrodeposited Thin Films of MoS_x. Although the photoelectrochemical reduction of $(NH_4)_2MoS_4$ on p-$GaInP_2$ can readily occur under a variety of conditions, this work highlights parameters necessary for thin, uniform films. First, a light intensity of 50 mW cm^{-2} white light was utilized, as full 1-sun illumination resulted in much thicker films, even for short deposition times. Second, $(NH_4)_2MoS_4$ concentrations on the order of 0.001 M were optimal. Higher concentrations resulted in strongly colored solutions that severely attenuated illumination. Lower concentrations resulted in sporadic, nonuniform deposits. Third, galvanostatic rather than voltammetric depositions yielded the most uniform films. Low current densities ($\sim 10^{-4}$ A cm^{-2}) also yielded the most continuous films. Higher current densities produced thicker (>60 nm) and rougher films, which incurred greater optical losses and correspondingly lower attainable photocurrents.

The as-photoelectrodeposited thin films were neither crystalline nor homogeneous in composition. The cumulative XP spectra and EELS mapping suggest these films are a mixture of MoS_2 and nonstoichiometric molybdenum sulfide, i.e., MoS_x. The data are presently unclear whether any oxysulfide forms natively during photoelectrodeposition. Additionally, the distribution of different Mo/S valence states (e.g., clustering) within the film is uncertain. However, the reactivity of the films toward oxygen would be consistent with the determination that the films are not strongly ordered. Crystalline features (e.g., Raman modes) only observed after some annealing imply that the photoelectrodeposition process yields a metastable form of MoS_x.

Still, a noteworthy feature of the photoelectrodeposition process was the apparent lack of Mo- and S-enrichment. This feature, in conjunction with the relative simplicity of the photoelectrodeposition process, stands in strong contrast to other methodologies for coating p-$GaInP_2$ with MoS_2-based coatings. A two-step Mo sputtering and the subsequent sulfidization process has been reported previously for modifying p-$GaInP_2$ that indicated it is difficult to fully convert Mo^0 films, especially at the interface.[16] Although the substoichiometry of the metal sulfide (and presence of Mo^0) apparently had minimal impact on the stability and catalytic activity of the electrode interface, the light-limited photocurrent was attenuated. This may signify an inherent limitation to the sulfidization process. That is, strong interactions between the Mo metal and the substrate, as well as the presence of coordinated oxygen could inhibit complete sulfidization within accepted thermal and temporal budgets.[41,42] Additionally, it is unclear whether sputtering damage occurs/impacts the performance of photoelectrodes during the catalyst deposition. Plasma damage to sputtering substrates and resulting films is well documented, where ion bombardment can create surface defects that impact electrical properties.[43−45] Regardless, those complications did not affect this work. The lack of Mo^0 and the ability to deposit optically thin films stand as major practical advantages of the method presented here. Although the simplicity of ambient electrodeposition apparatus relative to high-temperature equipment is well established at this point,[46] it merits further mentioning that ambient temperature deposition also avoids the interdiffusion problems associated with exposing the film/electrode to high temperatures.[28]

A further notable aspect observed here is the absence of substantial optical losses after coating. The near invariance in light-limited photocurrents in Figure 5a implies these coatings are essentially transparent to the incident illumination. Any deposited material with a refractive index between that of $GaInP_2$ and the liquid electrolyte will necessarily decrease the amount of incident illumination reflected. Although it is tempting to ascribe some additional light trapping between the film and p-$GaInP_2$ as the source for the slight photocurrent enhancement, replicate samples showed the same primary observation (i.e., the photocurrent magnitude was the same) but with no discernable enhancement. This observation could speak to slight variations in the specific refractive indices or absorbance between films and was not assessed further. Nevertheless, the principal fact that films, which were electrocatalytic, yielded no substantial changes in the reflectance, wavelength-dependent quantum yields for photocurrent, and the total white-light photocurrent is clear that the optical properties of the modified p-$GaInP_2$ photocathodes are well suited for water splitting. This point is especially true for multijunction photoelectrode architectures, where minimizing optical losses between layers is critical.[5,9,10]

DOI: 10.1021/acsami.9b03742
ACS Appl. Mater. Interfaces XXXX, XXX, XXX−XXX

Electrocatalytic Properties of MoS_x. The marked difference in the current-potential responses under illumination before and after the modification of p-$GaInP_2$ speaks strongly to the electrocatalytic nature of the as-prepared MoS_x films. That is, the as-prepared MoS_x films act as potent electrocatalysts for H^+ reduction. This point can be understood from the cumulative literature on the electrocatalytic nature of MoS_2. Simply, although crystalline MoS_2 is a layered material with extremely stable basal planes,[47,48] the most potent sites for H^+ adsorption and reduction are believed to be the undercoordinated Mo−S units at edge sites.[49−51] In fact, amorphous, heavily disordered, and defect-rich MoS_2 has been intentionally targeted as an ideal morphology of this sulfide for electrocatalysis.[31,34,50,52,53] These disordered MoS_2/MoS_x materials can exhibit exchange current densities upward of 10^{-5} A cm^{-2}, compared to 10^{-4} A cm^{-2} for Pt.[32,54] The onset potential for hydrogen evolution of MoS_x thin films deposited for 30 s in this work (0.68 and 0.62 V at 0.1 mA cm^{-2}) surpasses other $MoS_{2/x}$ films on p-$GaInP_2$ photocathodes (0.36[16] and ∼0.49[2] V at 0.1 mA cm^{-2}). Accordingly, these results suggest that the photoelectrodeposition process employed here also naturally yields a very active form of MoS_x.

Stability. The long operational life of the modified p-$GaInP_2$ electrodes is encouraging and noteworthy. The durability results shown here compare favorably to other MoS_x-modified photocathodes without additional protective oxide layers (Supporting Information, Table S1). Fundamentally, the stability of a photocathode immersed in water can be understood as a function of two (or more) current processes operating in parallel at the semiconductor/solution interface.[55] Concurrent to chemically induced corrosion processes, photogenerated electrons can either participate in the electrochemical reduction of species in the solution or in the electrochemical reduction of the semiconductor itself at the interface, with the relative fractions dictated by the "resistance" (i.e., kinetics) of the two current branches. In the absence of any electrocatalyst, the current flowing across a p-$GaInP_2$ electrode in water under hydrogen-evolving conditions quickly decreases, because the concurrent reduction of the group III elements to zero-valent metals is kinetically competitive with H^+ to H_2.[13,55−57] This aspect is clearly reflected in the rapid current loss in Figure 6 for the bare p-$GaInP_2$ photocathode. The substantially slower current decays of the p-$GaInP_2$ photocathodes modified by MoS_x reflect the fact that H^+ reduction became much more kinetically facile.

To be clear, the stability of these modified p-$GaInP_2$ electrodes is improved but by no means indefinite. Any loss in photocurrent indicates some finite, parallel degradation processes. Any residual Faradaic current not directed toward H_2 evolution will eventually lead to catastrophic failure if it is coupled to some corrosions of the photoelectrode.[56,57] A detailed analysis was not performed on the failure mechanisms of these films. Failure could involve the catalyst dissolution and/or poor catalyst adhesion. Although the stability of MoS_2 in water-splitting reactions is known,[18] molybdenum oxides are susceptible toward dissolution under hydrogen-evolving conditions,[58,59] exposing the underlying substrate. Accordingly, the elimination of any oxides in the film should be pursued to enhance the stability for much longer operating times. Additionally, the native surface oxide on $GaInP_2$ likely influences the adhesion of MoS_x. There is no reason a priori to believe that adhesion should be strong at this interface, but the evidence is clear that films adhere on the time scale of days. Specifically modifying $GaInP_2$ surfaces prior to photoelectrodeposition to enhance binding interactions with MoS_x may be required for much longer photoelectrolysis times. On this front, several routes for covalent modification of III−V semiconductor surfaces are known.[60,61]

CONCLUSIONS

The cumulative data show that the direct photoelectrodeposition of MoS_x thin films on p-$GaInP_2$ epilayers provides excellent catalytic activity and enhanced durability for photoelectrochemical hydrogen evolution. The key advancement demonstrated by this work is the ability to fabricate thin films on high efficiency III−V substrates with high catalytic performance and negligible photocurrent loss via an ambient benchtop electrodeposition requiring only aqueous solutions and simple electronics. A notable conclusion is that these films can stabilize otherwise corrosion-prone materials, setting the basis for future studies aimed at depositing other catalytically active, yet stable materials on photoelectrodes. From a practical standpoint, the fact that this stability enhancement was achieved without any other additional protection layer greatly simplifies the interface design. Nevertheless, controlling the interfacial chemistry of the $GaInP_2$ electrode before photoelectrodeposition may also prove useful in manipulating the film morphology for adjusting the deposit's optical properties or altering the system energetics for enhanced overall performance. The fact that the photoelectrodeposited films shown here already demonstrate 50 h of operation is encouraging, particularly given the ease and rapidity of their preparation.

ASSOCIATED CONTENT

Supporting Information

The Supporting Information is available free of charge on the ACS Publications website at DOI: 10.1021/acsami.9b03742.

2 min MoS_x photoelectrodeposition, EELS spectra and Mo EELS mapping data, replicate MoS_x depositions, and tabulated reference data (PDF)

AUTHOR INFORMATION

Corresponding Author

*E-mail: smald@umich.edu. Tel: 734-647-4750.

ORCID

Jun Liu: 0000-0003-0159-9767

Stephen Maldonado: 0000-0002-2917-4851

Notes

The authors declare no competing financial interest.

ACKNOWLEDGMENTS

M.L., Q.C., M.M.M., and S.M. acknowledge the generous support from the Department of Energy (DE-SC0006628). M.L. also acknowledges the U.S. Department of Energy, Office of Science, Office of Workforce Development for Teachers and Scientists for partial support of this work via the Graduate Student Research (SCGSR) program administered by the Oak Ridge Institute for Science and Education (DE-SC0014664). M.M.M. acknowledges the National Science Foundation (NSF) for the support through the Graduate Research Fellowship Program. The authors acknowledge the financial support and technical assistance from the Michigan Center for Materials Characterization under NSF grant number DMR-

DOI: 10.1021/acsami.9b03742
ACS Appl. Mater. Interfaces XXXX, XXX, XXX−XXX

0420785. The authors would also like to separately thank M. Steiner and W. Olavarria for preparing $GaInP_2$ epilayers. This work was authored in part by the National Renewable Energy Laboratory, operated by Alliance for Sustainable Energy, LLC, for the U.S. Department of Energy (DOE) under Contract No. DE-AC36-08GO28308. Funding was provided by the U.S. Department of Energy Office of Energy Efficiency and Renewable Energy Fuel Cell Technologies Office. The views expressed in the article do not necessarily represent the views of the DOE or the U.S. Government. The U.S. Government retains, and the publisher, by accepting the article for publication, acknowledges that the U.S. Government retains a nonexclusive, paid-up, irrevocable, worldwide license to publish or reproduce the published form of this work or allow others to do so, for U.S. Government purposes.

REFERENCES

(1) MacLeod, B. A.; Steirer, K. X.; Young, J. L.; Koldemir, U.; Sellinger, A.; Turner, J. A.; Deutsch, T. G.; Olson, D. C. Phosphonic Acid Modification of GaInP2 Photocathodes Toward Unbiased Photoelectrochemical Water Splitting. *ACS Appl. Mater. Interfaces* **2015**, *7*, 11346−11350.

(2) Gu, J.; Aguiar, J. A.; Ferrere, S.; Steirer, K. X.; Yan, Y.; Xiao, C. X.; Young, J. L.; Al-Jassim, M.; Neale, N. R.; Turner, J. A. A graded catalytic-protective layer for an efficient and stable water-splitting photocathode. *Nat. Energy* **2017**, *2*, No. 16192.

(3) Wang, H. L.; Deutsch, T.; Turner, J. A. Direct water splitting under visible light with nanostructured hematite and WO3 photoanodes and a GaInP2 photocathode. *J. Electrochem. Soc.* **2008**, *155*, F91−F96.

(4) Kocha, S. S.; Turner, J. A.; Nozik, A. J. Study of the Schottky-Barrier and Determination of the Energetic Positions of Band Edges at the n-Type and p-Type Gallium Indium-Phosphide Electrode-Electrolyte Interface. *J. Electroanal. Chem.* **1994**, *367*, 27−30.

(5) Young, J. L.; Steiner, M. A.; Doscher, H.; France, R. M.; Turner, J. A.; Deutsch, T. G. Direct solar-to-hydrogen conversion via inverted metamorphic multi-junction semiconductor architectures. *Nat. Energy* **2017**, *2*, No. 17028.

(6) Geisz, J. F.; Steiner, M. A.; Garcia, I.; Kurtz, S. R.; Friedman, D. J. Enhanced external radiative efficiency for 20.8% efficient single-junction GaInP solar cells. *Appl. Phys. Lett.* **2013**, *103*, No. 041118.

(7) Bertness, K. A.; Kurtz, S. R.; Friedman, D. J.; Kibbler, A. E.; Kramer, C.; Olson, J. M. 29.5-Percent-Efficient GaInP/GaAs Tandem Solar-Cells. *Appl. Phys. Lett.* **1994**, *65*, 989−991.

(8) Kocha, S. S.; Montgomery, D.; Peterson, M. W.; Turner, J. A. Photoelectrochemical decomposition of water utilizing monolithic tandem cells. *Sol. Energy Mater. Sol. Cells* **1998**, *52*, 389−397.

(9) Khaselev, O.; Turner, J. A. A monolithic photovoltaic-photoelectrochemical device for hydrogen production via water splitting. *Science* **1998**, *280*, 425−427.

(10) May, M. M.; Lewerenz, H. J.; Lackner, D.; Dimroth, F.; Hannappel, T. Efficient direct solar-to-hydrogen conversion by in situ interface transformation of a tandem structure. *Nat. Commun.* **2015**, *6*, No. 8286.

(11) Bansal, A.; Turner, J. A. Suppression of band edge migration at the p-GaInP2/H2O interface under illumination via catalysis. *J. Phys. Chem. B* **2000**, *104*, 6591−6598.

(12) Wang, H.; Deutsch, T.; Welch, A.; Turner, J. A. The stability of illuminated p-GaInP2 semiconductor photoelectrode. *Int. J. Hydrogen Energy* **2012**, *37*, 14009−14014.

(13) Khaselev, O.; Turner, J. A. Electrochemical stability of p-GaInP2 in aqueous electrolytes toward photoelectrochemical water splitting. *J. Electrochem. Soc.* **1998**, *145*, 3335−3339.

(14) Kocha, S. S.; Turner, J. A. Displacement of the Band edges of GaInP2 in Aqueous-Electrolytes Induced by Surface Modification. *J. Electrochem. Soc.* **1995**, *142*, 2625−2630.

(15) Kocha, S. S.; Peterson, M. W.; Nelson, A. J.; Rosenwaks, Y.; Arent, D. J.; Turner, J. A. Investigation of Chemical Wet-Etch Surface Modification of Ga0.5in0.5p Using Photoluminescence, X-Ray Photoelectron-Spectroscopy, Capacitance Measurements, and Photocurrent-Voltage Curves. *J. Phys. Chem. A* **1995**, *99*, 744−749.

(16) Britto, R. J.; Benck, J. D.; Young, J. L.; Hahn, C.; Deutsch, T. G.; Jaramillo, T. F. Molybdenum Disulfide as a Protection Layer and Catalyst for Gallium Indium Phosphide Solar Water Splitting Photocathodes. *J. Phys. Chem. Lett.* **2016**, *7*, 2044−2049.

(17) Sun, K.; Saadi, F. H.; Lichterman, M. F.; Hale, W. G.; Wang, H. P.; Zhou, X. H.; Plymale, N. T.; Omelchenko, S. T.; He, J. H.; Papadantonakis, K. M.; Brunschwig, B. S.; Lewis, N. S. Stable solar-driven oxidation of water by semiconducting photoanodes protected by transparent catalytic nickel oxide films. *Proc. Natl. Acad. Sci. U.S.A.* **2015**, *112*, 3612−3617.

(18) Laursen, A. B.; Pedersen, T.; Malacrida, P.; Seger, B.; Hansen, O.; Vesborg, P. C. K.; Chorkendorff, I. MoS2-an integrated protective and active layer on n(+)p-Si for solar H-2 evolution. *Phys. Chem. Chem. Phys.* **2013**, *15*, 20000−20004.

(19) Gu, J.; Yan, Y.; Young, J. L.; Steirer, K. X.; Neale, N. R.; Turner, J. A. Water reduction by a p-GaInP2 photoelectrode stabilized by an amorphous TiO2 coating and a molecular cobalt catalyst. *Nat. Mater.* **2016**, *15*, 456−460.

(20) Hu, S.; Shaner, M. R.; Beardslee, J. A.; Lichterman, M.; Brunschwig, B. S.; Lewis, N. S. Amorphous TiO2 coatings stabilize Si, GaAs, and GaP photoanodes for efficient water oxidation. *Science* **2014**, *344*, 1005−1009.

(21) Zhou, X. H.; Liu, R.; Sun, K.; Papadantonakis, K. M.; Brunschwig, B. S.; Lewis, N. S. 570 mV photovoltage, stabilized n-Si/CoOx heterojunction photoanodes fabricated using atomic layer deposition. *Energy Environ. Sci.* **2016**, *9*, 892−897.

(22) Rovelli, L.; Tilley, S. D.; Sivula, K. Optimization and Stabilization of Electrodeposited Cu2ZnSnS4 Photocathodes for Solar Water Reduction. *ACS Appl. Mater. Interfaces* **2013**, *5*, 8018−8024.

(23) Xu, Y. F.; Wang, X. D.; Chen, H. Y.; Kuang, D. B.; Su, C. Y. Toward High Performance Photoelectrochemical Water Oxidation: Combined Effects of Ultrafine Cobalt Iron Oxide Nanoparticle. *Adv. Funct. Mater.* **2016**, *26*, 4414−4421.

(24) Xiao, J. R.; Huang, H. L.; Huang, Q. Y.; Li, X.; Hou, X. L.; Zhao, L.; Ma, R.; Chen, H.; Li, Y. D. Remarkable improvement of the turn-on characteristics of a Fe2O3 photoanode for photoelectrochemical water splitting with coating a FeCoW oxy-hydroxide gel. *Appl. Catal., B* **2017**, *212*, 89−96.

(25) Prabhakar, R. R.; Septina, W.; Siol, S.; Moehl, T.; Wick-Joliat, R.; Tilley, S. D. Photocorrosion-resistant Sb2Se3 photocathodes with earth abundant MoSx hydrogen evolution catalyst. *J. Mater. Chem. A* **2017**, *5*, 23139−23145.

(26) Morales-Guio, C. G.; Liardet, L.; Mayer, M. T.; Tilley, S. D.; Gratzel, M.; Hu, X. L. Photoelectrochemical Hydrogen Production in Alkaline Solutions Using Cu2O Coated with Earth-Abundant Hydrogen Evolution Catalysts. *Angew. Chem.* **2015**, *127*, 674−677.

(27) Kageshima, Y.; Minegishi, T.; Sugisaki, S.; Goto, Y.; Kaneko, H.; Nakabayashi, M.; Shibata, N.; Domen, K. Surface Protective and Catalytic Layer Consisting of RuO2 and Pt for Stable Production of Methylcyclohexane Using Solar Energy. *ACS Appl. Mater. Interfaces* **2018**, *10*, 44396−44402.

(28) Francis, C.; Bradley, M. A.; Boucaud, P.; Julien, F. H.; Razeghi, M. Intermixing of GaInP/GaAs Multiple Quantum-Wells. *Appl. Phys. Lett.* **1993**, *62*, 178−180.

(29) Lita, B.; Goldman, R. S.; Phillips, J. D.; Bhattacharya, P. K. Interdiffusion and surface segregation in stacked self-assembled InAs/GaAs quantum dots. *Appl. Phys. Lett.* **1999**, *75*, 2797−2799.

(30) Pearton, S. J.; Malm, D. L.; Heimbrook, L. A.; Kovalchick, J.; Abernathy, C. R.; Caruso, R.; Vernon, S. M.; Haven, V. E. Heterointerface Stability in GaAs-on-Si Grown by Metalorganic Chemical Vapor-Deposition. *Appl. Phys. Lett.* **1987**, *51*, 682−684.

(31) Benck, J. D.; Chen, Z. B.; Kuritzky, L. Y.; Forman, A. J.; Jaramillo, T. F. Amorphous Molybdenum Sulfide Catalysts for

DOI: 10.1021/acsami.9b03742
ACS Appl. Mater. Interfaces XXXX, XXX, XXX−XXX

Electrochemical Hydrogen Production: Insights into the Origin of their Catalytic Activity. *ACS Catal.* **2012**, *2*, 1916−1923.
(32) Merki, D.; Hu, X. L. Recent developments of molybdenum and tungsten sulfides as hydrogen evolution catalysts. *Energy Environ. Sci.* **2011**, *4*, 3878−3888.
(33) Deng, Y. L.; Ting, L. R. L.; Neo, P. H. L.; Zhang, Y. J.; Peterson, A. A.; Yeo, B. S. Operando Raman Spectroscopy of Amorphous Molybdenum Sulfide (MoSx) during the Electrochemical Hydrogen Evolution Reaction: Identification of Sulfur Atoms as Catalytically Active Sites for H+ Reduction. *ACS Catal.* **2016**, *6*, 7790−7798.
(34) Merki, D.; Fierro, S.; Vrubel, H.; Hu, X. L. Amorphous molybdenum sulfide films as catalysts for electrochemical hydrogen production in water. *Chem. Sci.* **2011**, *2*, 1262−1267.
(35) Barr, T. L.; Seal, S. Nature of the Use of Adventitious Carbon as a Binding-Energy Standard. *J. Vac. Sci. Technol., A* **1995**, *13*, 1239−1246.
(36) Vrubel, H.; Hu, X. L. Growth and Activation of an Amorphous Molybdenum Sulfide Hydrogen Evolving Catalyst. *ACS Catal.* **2013**, *3*, 2002−2011.
(37) Ponomarev, E. A.; Neumann-Spallart, M.; Hodes, G.; Levy-Clement, C. Electrochemical deposition of MoS2 thin films by reduction of tetrathiomolybdate. *Thin Solid Films* **1996**, *280*, 86−89.
(38) Benoist, L.; Gonbeau, D.; Pfisterguillouzo, G.; Schmidt, E.; Meunier, G.; Levasseur, A. X-Ray Photoelectron-Spectroscopy Characterization of Amorphous Molybdenum Oxysulfide Thin-Films. *Thin Solid Films* **1995**, *258*, 110−114.
(39) Cheong, H. M.; Mascarenhas, A.; Ernst, P.; Geng, C. Effects of spontaneous ordering on Raman spectra of GaInP2. *Phys. Rev. B* **1997**, *56*, 1882−1887.
(40) Li, H.; Zhang, Q.; Yap, C. C. R.; Tay, B. K.; Edwin, T. H. T.; Olivier, A.; Baillargeat, D. From Bulk to Monolayer MoS2: Evolution of Raman Scattering. *Adv. Funct. Mater.* **2012**, *22*, 1385−1390.
(41) Spevack, P. A.; Mcintyre, N. S. A Raman and Xps Investigation of Supported Molybdenum Oxide Thin-Films .2. Reactions with Hydrogen-Sulfide. *J Phys. Chem.* **1993**, *97*, 11031−11036.
(42) Lee, B. S.; Rapp, R. A. Gaseous Sulfidation of Pure Molybdenum at 700-Degrees-C-950-Degrees-C. *J. Electrochem. Soc.* **1984**, *131*, 2998−3006.
(43) Fonash, S. J.; Ashok, S.; Singh, R. Effect of Ion-Beam Sputter Damage on Schottky-Barrier Formation in Silicon. *Appl. Phys. Lett.* **1981**, *39*, 423−425.
(44) Kim, H. K.; Lee, K. S.; Kwon, J. H. Transparent indium zinc oxide top cathode prepared by plasma damage-free sputtering for top-emitting organic light-emitting diodes. *Appl. Phys. Lett.* **2006**, *88*, No. 012103.
(45) Kelly, P. J.; Arnell, R. D. Magnetron sputtering: a review of recent developments and applications. *Vacuum* **2000**, *56*, 159−172.
(46) Fahrenkrug, E.; Maldonado, S. Electrochemical Liquid-Liquid-Solid (ec-LLS) Crystal Growth: A Low-Temperature Strategy for Covalent Semiconductor Crystal Growth. *Acc. Chem. Res.* **2015**, *48*, 1881−1890.
(47) Fleischauer, P. D. Effects of Crystallite Orientation on Environmental Stability and Lubrication Properties of Sputtered MoS2 Thin-Films. *ASLE Trans.* **1984**, *27*, 82−88.
(48) Parzinger, E.; Miller, B.; Blaschke, B.; Garrido, J. A.; Ager, J. W.; Holleitner, A.; Wurstbauer, U. Photocatalytic Stability of Single- and Few-Layer MoS2. *ACS Nano* **2015**, *9*, 11302−11309.
(49) Li, G. Q.; Zhang, D.; Qiao, Q.; Yu, Y. F.; Peterson, D.; Zafar, A.; Kumar, R.; Curtarolo, S.; Hunte, F.; Shannon, S.; Zhu, Y. M.; Yang, W. T.; Cao, L. Y. All The Catalytic Active Sites of MoS2 for Hydrogen Evolution. *J. Am. Chem. Soc.* **2016**, *138*, 16632−16638.
(50) Xie, J. F.; Zhang, H.; Li, S.; Wang, R. X.; Sun, X.; Zhou, M.; Zhou, J. F.; Lou, X. W.; Xie, Y. Defect-Rich MoS2 Ultrathin Nanosheets with Additional Active Edge Sites for Enhanced Electrocatalytic Hydrogen Evolution. *Adv. Mater.* **2013**, *25*, 5807−5813.
(51) Wu, Z. Z.; Fang, B. Z.; Wang, Z. P.; Wang, C. L.; Liu, Z. H.; Liu, F. Y.; Wang, W.; Alfantazi, A.; Wang, D. Z.; Wilkinson, D. P. MoS2 Nanosheets: A Designed Structure with High Active Site Density for the Hydrogen Evolution Reaction. *ACS Catal.* **2013**, *3*, 2101−2107.
(52) Ye, G.; Gong, Y. J.; Lin, J. H.; Li, B.; He, Y. M.; Pantelides, S. T.; Zhou, W.; Vajtai, R.; Ajayan, P. M. Defects Engineered Monolayer MoS2 for Improved Hydrogen Evolution Reaction. *Nano Lett.* **2016**, *16*, 1097−1103.
(53) Tan, J.; Yang, W.; Oh, Y.; Lee, H.; Park, J.; Moon, J. Controlled Electrodeposition of Photoelectrochemically Active Amorphous MoSx Cocatalyst on Sb2Se3 Photocathode. *ACS Appl. Mater. Interfaces* **2018**, *10*, 10898−10908.
(54) Sheng, W. C.; Gasteiger, H. A.; Shao-Horn, Y. Hydrogen Oxidation and Evolution Reaction Kinetics on Platinum: Acid vs Alkaline Electrolytes. *J. Electrochem. Soc.* **2010**, *157*, B1529−B1536.
(55) Gerischer, H. Stability of Semiconductor Electrodes against Photodecomposition. *J. Electroanal. Chem. Interfacial Electrochem.* **1977**, *82*, 133−143.
(56) Brown, E. S.; Peczonczyk, S. L.; Wang, Z. J.; Maldonado, S. Photoelectrochemical Properties of CH3-Terminated p-Type GaP(111)A. *J. Phys. Chem. C* **2014**, *118*, 11593−11600.
(57) Butler, M. A.; Ginley, D. S. P-Type GaP as a Semiconducting Photoelectrode. *J. Electrochem. Soc.* **1980**, *127*, 1273−1278.
(58) Saji, V. S.; Lee, C. W. Molybdenum, Molybdenum Oxides, and their Electrochemistry. *ChemSusChem* **2012**, *5*, 1146−1161.
(59) Chen, Z. B.; Cummins, D.; Reinecke, B. N.; Clark, E.; Sunkara, M. K.; Jaramillo, T. F. Core-shell MoO3-MoS2 Nanowires for Hydrogen Evolution: A Functional Design for Electrocatalytic Materials. *Nano Lett.* **2011**, *11*, 4168−4175.
(60) Garner, L. E.; Steirer, K. X.; Young, J. L.; Anderson, N. C.; Miller, E. M.; Tinkham, J. S.; Deutsch, T. G.; Sellinger, A.; Turner, J. A.; Neale, N. R. Covalent Surface Modification of Gallium Arsenide Photocathodes for Water Splitting in Highly Acidic Electrolyte. *ChemSusChem* **2017**, *10*, 767−773.
(61) Peczonczyk, S. L.; Mukherjee, J.; Carim, A. I.; Maldonado, S. Wet Chemical Functionalization of III-V Semiconductor Surfaces: Alkylation of Gallium Arsenide and Gallium Nitride by a Grignard Reaction Sequence. *Langmuir* **2012**, *28*, 4672−4682.

DOI: 10.1021/acsami.9b03742
ACS Appl. Mater. Interfaces XXXX, XXX, XXX−XXX